Effect of Ce and Zr codoping on the multiferroic properties of $BiFeO_3$ thin films

2010 EPL 89 57004

(http://iopscience.iop.org/0295-5075/89/5/57004)

A Letters Journal Exploring the Frontiers of Physics

March 2010

EPL, **89** (2010) 57004
doi: 10.1209/0295-5075/89/57004

www.epljournal.org

Effect of Ce and Zr codoping on the multiferroic properties of $BiFeO_3$ thin films

Jun Liu, Meiya Li[a], Ling Pei, Jing Wang, Zhongqiang Hu, Xiao Wang and Xingzhong Zhao

Department of Electronic Science and Technology, School of Physical Science and Technology, Wuhan University Wuhan 430072, PRC
Key Laboratory of Acoustic and Photonic Material and Device of the Ministry of Education, Wuhan University Wuhan 430072, PRC

received 27 October 2009; accepted in final form 17 February 2010
published online 23 March 2010

PACS 77.80.-e – Ferroelectricity and antiferroelectricity

Abstract – Pure $BiFeO_3$(BFO), Ce-doped $BiFeO_3$(BCFO), Zr-doped $BiFeO_3$(BFZO), as well as Ce- and Zr-codoped $BiFeO_3$(BCFZO) thin films were successfully prepared on $Pt/Ti/SiO_2/Si$ substrates by chemical solution deposition. The effects of Ce and Zr doping on the structure, surface morphology, electrical and magnetic properties of BFO films were studied. X-ray diffraction and atomic force microscopy analysis revealed structure transition and decreased grain sizes in the doped BFO films. In comparison with the other doped BFO films studied here, the Ce- and Zr-codoped BCFZO film showed the lowest dielectric loss and leakage current density and exhibited a well-squared hysteresis loop with a remanent polarization P_r of $64\,\mu C/cm^2$ and a coercive electric field E_c of 339 kV/cm, as well as the fatigue-free characteristics. Meanwhile, the largest magnetization was also observed in this codoped film. The possible reasons for the enhancement of the ferroelectricity and the ferromagnetism of these films were discussed.

Multiferroic materials that show ferroelectric and ferromagnetic ordering simultaneously are currently attracting significant attention due to their interesting fundamental physics as well as the potential applications [1–4]. Among the single-phase multiferroic materials studied so far, $BiFeO_3$, with a rhombohedrally distorted perovskite structure with space group $R3c$, is the only one that exhibits both ferroelectricity and G-type anti-ferromagnetism at room temperature (with Curie temperature $T_C \sim 1103$ K and Néel temperature $T_N \sim 643$ K), which makes it the most appropriate for applications at room temperature [5,6].

However, pure BFO has a serious high-leakage-current problem resulting from charge defects such as oxygen vacancies, which makes it hard to gain good ferroelectricity [7]. Besides, the spatial periodic inhomogeneous spin structure of BFO leads to the cancellation of the ion magnetic moments [6,8,9]. These problems hindered its practical applications in multiferroic devices. To improve the properties of BFO, considerable efforts have been made, for instance, Bi-site substitution with Nd^{3+}, Gd^{3+} and Pr^{4+} [10–12] and Fe-site substitution with Ni^{2+}, Cr^{3+}, Ti^{4+}, Zr^{4+} and Nb^{5+} [13–17]. Since the ferroelectricity and magnetism of BFO come from the lone pair electrons of Bi^{3+} ions and the magnetism of Fe^{3+} ions, respectively [4], to further improve the multiferroic properties of BFO, Bi-site and Fe-site codoping has attracted great interest. Seung U. Lee *et al.* [18] reported that Nd^{3+} and Cr^{3+} codoping as well as Sm^{3+} and Cr^{3+} codoping in BFO films not only reduced the leakage current but also improved the ferroelectric properties of the films. Chia-ching Lee *et al.* [19] found that La^{3+} and Ti^{4+} codoping reduced both the leakage current and the relaxation gap of the P-E hysteresis loop of the BFO film. Zhenxiang Cheng *et al.* [20] observed that La^{3+} and Nb^{5+} codoping in a BFO film effectively improved the dielectric and ferroelectric properties of the film. Bengfang Yu *et al.* [21] revealed that La^{3+} and V^{5+} codoping decreased the leakage current and enhanced the dielectricity of BFO ceramics. However, few work related to the magnetic properties of a codoped BFO film was reported. Recently, our study revealed that the A-site Ce-doped BFO films had improved ferroelectric properties [22]. Considering the fact that the valence of Zr^{4+} is higher than that of Fe^{3+} and the ionic radius of Zr^{4+} (0.072 nm) is larger than that of Fe^{3+} (0.064 nm) [21], it is expected that the high-valence

[a]E-mail: myli@whu.edu.cn

Zr^{4+} substitution for the Fe^{3+} at the B-site could fill the oxygen vacancies induced by the possible transition from Fe^{3+} to Fe^{2+} and suppress the inhomogeneous magnetic spin structure to improve the magnetic properties of the BFO film. Therefore, in this paper, we chose the Ce and Zr ions, respectively, to substitute for the Bi and Fe ions in the BFO films prepared on $Pt/Ti/SiO_2/Si$ substrates by chemical solution deposition (CSD), and investigate the influences of codoping on the structure, surface morphology and multiferroic properties of the films.

The precursor solutions used in CSD were prepared by dissolving bismuth nitrate $[Bi(NO_3)_3 \cdot 5H_2O]$, iron nitrate $[Fe(NO_3)_3 \cdot 9H_2O]$, cerium nitrate $[Ce(NO_3)_3 \cdot 9H_2O]$ and zirconium nitrate $[Zr(NO_3)_4 \cdot 3H_2O]$ in a mixed solution of acetic acid and 2-methoxyethanol to form the final products with nominal compositions $BiFeO_3$ (BFO), $Bi_{0.97}Ce_{0.03}FeO_3$ (BCFO), $BiFe_{0.97}Zr_{0.03}O_3$ (BFZO), and $Bi_{0.97}Ce_{0.03}Fe_{0.97}Zr_{0.03}O_3$ (BCFZO). Five mol% of excess Bi was added to compensate the bismuth loss during the heat treatment. The solutions were spin coated on the $Pt/Ti/SiO_2/Si$ substrates at 3500 rpm for 20 s and dried at 150 °C for 5 min, and then pre-fired at 350 °C for 10 min in air. This process was repeated several times to obtain the desired film thickness. Then the films were annealed at 600 °C for 10 min in an oxygen atmosphere for crystallization. To measure the electrical properties of the films, circular Pt electrodes with an area of $3.14 \times 10^{-4}\,cm^2$ were fabricated on the surface of the films by rf-magnetron sputtering.

The structure of the films was analyzed by a X-ray diffractometer (D8 Advance, Bruker, German) with Cu K_α radiation. The surface morphology was observed by an atomic force microscope (AFM, SPM-9500J3). The dielectric constants and losses of these films were measured using an Agilent 4294A precision impedance analyzer. The leakage current, ferroelectric properties, and anti-fatigue properties of these films were measured by a ferroelectric test system (Precision Premier Workstation, Radiant Technology, USA). The magnetic properties of these films were measured by a physical property measurement system (PPMS, Quantum Design, USA). The oxidation status of Fe of these films was analyzed by X-ray photoelectron spectroscopy (XPS). All of these measurements were carried out at room temperature.

Figure 1 shows the XRD patterns of the BFO, BCFO, BFZO and BCFZO thin films. All the films show single-phase polycrystalline perovskite structure and, within the detectable limitation, no trace of impurities such as the magnetic oxide impurities γ-Fe_2O_3 etc. The intensity of the (110) diffraction peak of the BFO film is stronger than that of the (012) peak, suggesting a partly preferred orientation of the film along the (110) direction. However, with the (110) diffraction peak turning weak and the (012) diffraction peak becoming strong, these Ce- and Zr-doped BFO films show mixed orientation. To further investigate the influence of Ce and Zr doping on the structure of the BFO films, the subtle XRD patterns in the 2θ range

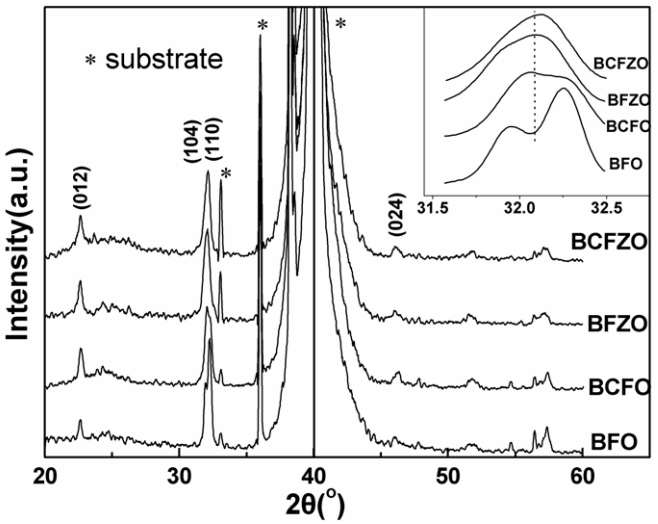

Fig. 1: XRD patterns of the BFO, BCFO, BFZO and BCFZO thin films, where the inset shows the magnified patterns in the vicinity of $2\theta = 32°$.

of 31.5°–32.5° are given. As can be seen in the inset of fig. 1, two clearly separated reflection peaks of (104) and (110) (indexed by the rhombohedral structure) in the vicinity of $2\theta = 32°$ in the pattern of the pure BFO film were merged into a single peak (110) (indexed by the tetragonal structure) in the pattern of the BCFO film, revealing a structure transition from rhombohedral to pseudotetragonal. This is in accordance with our previous report for the Ce-doped BFO films [22]. Likewise, the single peak in the vicinity of $2\theta = 32°$ in the patterns of the BFZO and BCFZO films suggests that the same structure transition may have happened in these films due to Zr doping and Ce-Zr codoping. Similar phenomena were also observed in the Nd-, Gd- and Zr-doped BFO films [10,11,16]. Compared with that of the pure BFO film, the single peak in the patterns of the BCFO and BFZO films has a tendency to shift towards higher and lower 2θ angle, respectively, while the single peak in the pattern of the BCFZO has no obvious shift. These peak shifts may suggest lattice distortions of the films and might be related to the fact that the ionic radii of Ce ions (Ce^{3+}(0.101 nm), Ce^{4+}(0.087 nm)) are smaller than that of Bi^{3+}(0.103 nm) but the ionic radius of Zr^{4+}(0.072 nm) is larger than that of Fe^{3+}(0.064 nm) [23].

Figure 2 presents the surface morphologies of the BFO, BCFO, BFZO and BCFZO thin films. Among these films, the pure BFO film has the largest grain sizes, while the Ce-doped BCFO film consists of the smallest grains with fine grains embedded among them. The BCFZO film has smaller grain size than those of the BFO and BFZO films and exhibits a very dense morphology without interstices. Similar morphologies have been observed in the Gd- and Ti-doped BFO films [7,11]. These morphologies might be related to the possible different crystallization temperatures of these films induced by the different chemical bond strength of

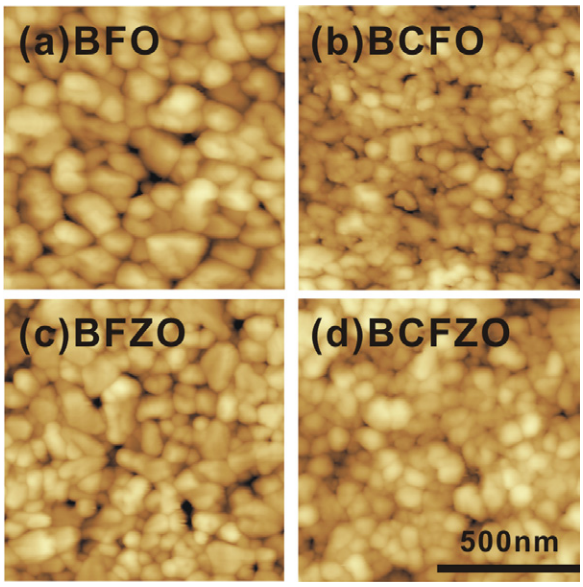

Fig. 2: (Colour on-line) AFM images of BFO, BCFO, BFZO and BCFZO thin films.

Ce–O, Zr–O, Bi–O, and Fe–O which relate directly to the melting temperatures of CeO_2(2600 °C), ZrO_2(2700 °C), Bi_2O_3(820 °C) and Fe_2O_3(1573 °C) [19,24], respectively. The thickness of all the films is about 425 ± 10 nm according to the cross-section morphologies (not shown here) of the samples observed by a scanning electron microscope.

Figure 3 illustrates the frequency dependences of the dielectric constants (ε_r) and dielectric losses ($\tan\delta$) of the BFO, BCFO, BFZO and BCFZO thin films. The ε_r values of all the films show only slight changes over the whole frequency ranging from 40 Hz to 1 MHz, whereas the ε_r values of the BCFO, BFZO and BCFZO films are much larger than that of the pure BFO film. The $\tan\delta$ values of the doped BFO films are smaller than that of the pure BFO film, among which the BCFZO film shows the smallest $\tan\delta$ value. These values suggest that the Ce and Zr codoping could increase the dielectric constant and reduce the dielectric loss and, therefore, improve the dielectric properties of the BFO film. This improvement may be attributed to the fact that the Ce and Zr codoping reduced the moveable charge defects and the thickness of the dielectric dead layer of the low dielectric constant existing at the interface between the film and the electrode [25].

Figure 4 exhibits the dependence of the leakage current density (J) on the applied electric field (E) for the BFO, BCFO, BFZO and BCFZO thin films. The BFO film exhibits a relatively high-leakage-current density, while the Ce- and Zr-codoped BCFZO film has the lowest-leakage-current density. Under an applied electric field of 200 kV/cm, the leakage current density of the BCFZO film is about 7.6×10^{-5} A/cm^2, which is approximately two and three orders of magnitude less than that of the BCFO (1.1×10^{-3} A/cm^2) and the BFO (2.6×10^{-2} A/cm^2) films, respectively. This indicates that the

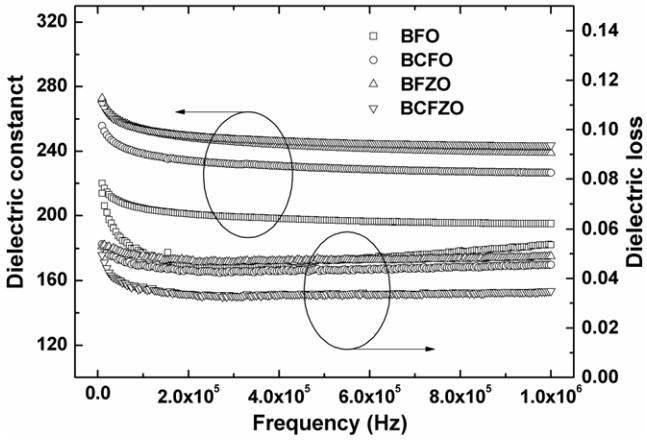

Fig. 3: ε_r and $\tan\delta$ of the BFO, BCFO, BFZO and BCFZO thin films as a function of frequencies.

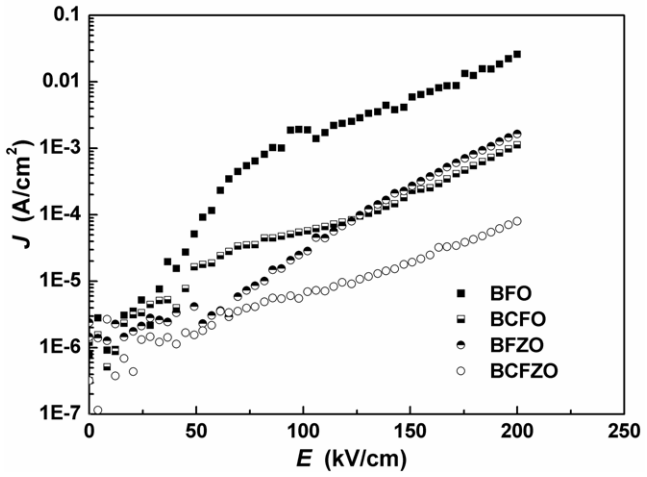

Fig. 4: Leakage current density (J) *vs.* electric field (E) for the BFO, BCFO, BFZO and BCFZO thin films.

Ce and Zr codoping greatly reduced the leakage current density of the BFO films, which is consistent with the lowest dielectric losses of the sample discussed above. It is well known that the high-leakage-current density in the pure BFO film originates mainly from charge defects such as oxygen vacancies which may come from the volatility of bismuth and the transition from Fe^{3+} to Fe^{2+} [7]. The Ce^{3+} substitution, especially the high-valence Ce^{4+} substitution for the volatile Bi^{3+} at the A-site in the BCFO film would suppress the formation of oxygen vacancies and reduce the density of oxygen vacancies [12,22]. While at the B-site, the high-valence Zr^{4+} substitution for Fe^{3+} would cause the filling of oxygen vacancies which might be induced by the transition from Fe^{3+} to Fe^{2+} [16]. Therefore, the codoping of the Ce ions and the Zr^{4+} could effectively eliminate the oxygen vacancies and thus reduce the leakage current density of the BFO film. In addition, the smaller grain size and denser morphology of the BCFZO film observed by AFM should also be favorable to the low-leakage-current density of the film [11].

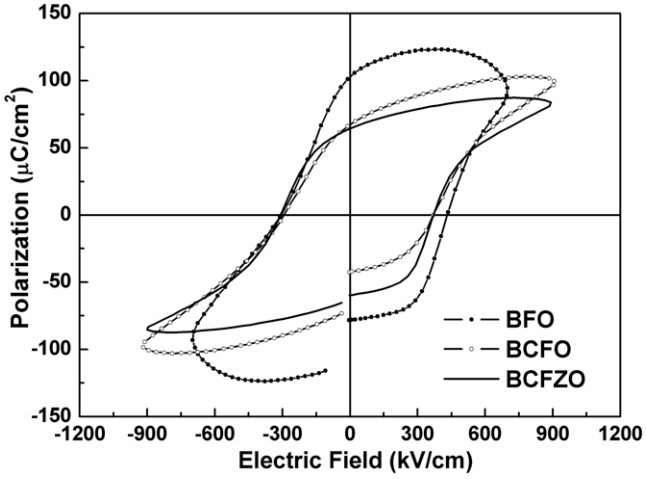

Fig. 5: *P-E* hysteresis loops of the BFO, BCFO and BCFZO thin films.

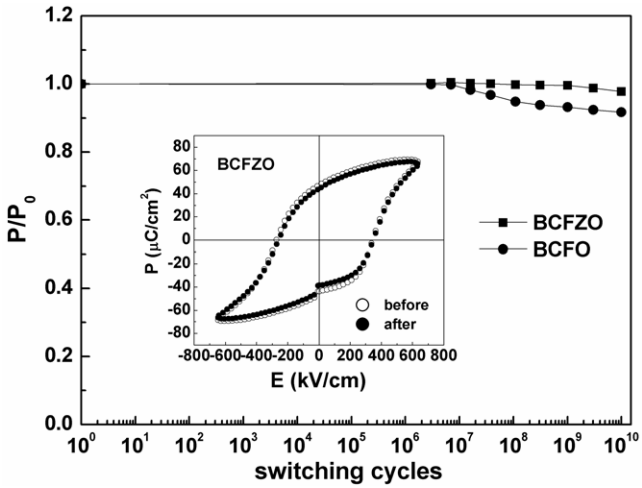

Fig. 6: Fatigue measurement of the BCFO and BCFZO thin films.

The ferroelectric hysteresis loops (*P-E* loops) of the BFO, BCFO, BFZO and BCFZO thin films are presented in fig. 5. The pure BFO film exhibits a poor *P-E* loop as evidenced by the rounded tips and the large relaxation gap, which could be ascribed to the contribution of the charge defects in the film [19,20]. This is consistent with the high-leakage-current density of this film discussed above. The BCFO film has a better *P-E* loop with a less rounded feature which means the contribution from the charge defects is significantly reduced. However, the relaxation gap is still observed in it. In spite of the low-leakage-current density of the BFZO film, it displays a worse *P-E* loop (not shown here). This may related to the transition from Fe^{3+} to Fe^{2+} induced by the high-valence Zr^{4+} substitution due to the charge neutrality and then the formation of the negatively charged defect $(Fe^{2+}_{Fe^{3+}})'$. Thus, in the material with oxygen vacancy, high content defect complexes of $(Fe^{2+}_{Fe^{3+}})'$-$(V_{O^{2-}})^{\bullet\bullet}$ may be formed by the electrostatic attraction force. The local internal fields produced by these defect complexes may provide a driving force for domain backswitching, leading to the fact that the domains in the BFZO film are difficult to be switched [26,27] and, therefore, a poor *P-E* loop was observed. Similar phenomena have been observed in the B-site high-valence Ti- [15] and Nb- [17] doped BFO films. However, under an applied electric field of 933 kV/cm, the BCFZO film shows a much better square-shaped *P-E* loop with a remanent polarization P_r of 64 μC/cm^2 and a coercive electric field E_c of 339 kV/cm. This improvement in ferroelectric properties could be attributed to the low-leakage-current density originating from the possible low-charge defects due to Ce and Zr codoping.

The fatigue behavior of the BCFO and BCFZO thin films at a frequency of 1 MHz is depicted in fig. 6, in which the inset shows the *P-E* loops of the BCFZO films before and after the fatigue test under an applied electric field of 667 kV/cm. The pure BFO film gets broken down under the applied measured electric field and no fatigue curve was obtained, suggesting a poor-fatigue property in comparison with the doped samples. This poor-fatigue property of the pure BFO was also demonstrated in our study for the Ce-doped BCFO film [28]. After being subjected to 1×10^{10} switching cycles, the remanent polarization of the BCFO film decreased by 8%, while the BCFZO film displays the best anti-fatigue behavior with 2Pr dropped by only 2%. As seen in the inset of fig. 6, the initial *P-E* loop of the BCFZO film coincides well with the one after being subjected to the whole fatigue cycles. This suggests that the Ce and Zr codoping could effectively improve the fatigue resistance of the BFO film. It is thought that several factors including domain wall pinning by the oxygen vacancies and the formation of interfacial layers at the electrode/ferroelectric interface were responsible for the polarization fatigue of the films [17,20]. As was indicated above, the Ce and Zr codoping could effectively reduce the oxygen vacancy density of the BFO film. Thereby, the Ce and Zr codoping would reduce the effect of domain walls pinning and the thickness of the interfacial layer, and thus improve the anti-fatigue property of the film.

The magnetic hysteresis (*M-H*) loops of the BFO, BCFO, BFZO and BCFZO thin films were measured using a PPMS with the magnetic field applied in parallel with the film surface, as shown in fig. 7. The diamagnetic contribution from the substrate was subtracted from the raw data. All the films demonstrate a weak ferromagnetic behavior, with saturated magnetizations (M_s) of 0.2 emu/cm^3, 0.5 emu/cm^3, 0.8 emu/cm^3 and 1.0 emu/cm^3 for the BFO, BCFO, BFZO and BCFZO films at a measuring magnetic field of 15 kOe, respectively. Although these values are smaller than that of the BFO films reported by Eerenstein *et al.* [2] which may result from the differences in preparing conditions, they clearly suggest that the Ce and Zr codoping has enhanced the magnetic

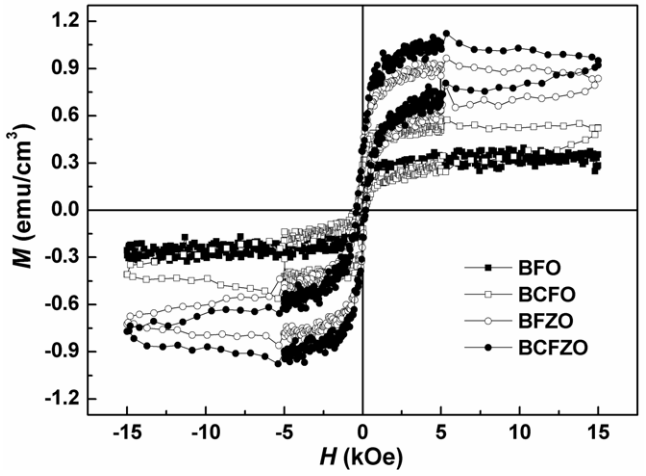

Fig. 7: M-H hysteresis loops of the BFO, BCFO, BFZO and BCFZO thin films.

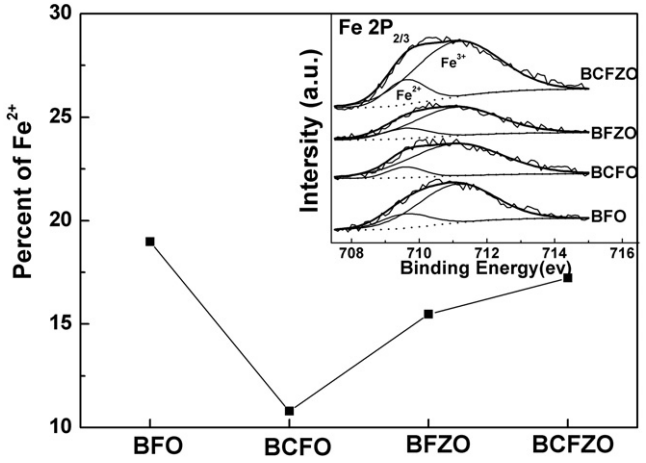

Fig. 8: The dependence of the Fe^{2+} content on the doping elements. The inset shows typical Fe $2P_{3/2}$ XPS spectra of the BFO, BCFO, BFZO and BCFZO thin films.

properties of the BFO films effectively. Due to the fact that the average grain size of all the films is larger than the period of the spin cycloid of BFO, the reasons for the enhancement of the magnetization should be not related to the grain sizes. The main factors affecting the magnetization of the films are discussed below. The enhancement of magnetization in BFO-based materials is usually ascribed to the formation of Fe^{2+} which would possibly cause a double-exchange interaction between Fe^{2+} and Fe^{3+} through oxygen [7,10]. In order to identify the origins of the increase of M_s in the BCFZO film, the XPS measurement was performed to investigate the oxidation of Fe, as shown in fig. 8. From the inset, the experimental Fe $2P_{3/2}$ band can be fitted well and the percentage of Fe^{2+} to the total Fe is 19%, 11%, 15% and 17% for the BFO, BCFO, BFZO and BCFZO films, respectively. This indicates that the Ce and Zr doping decreased the content of Fe^{2+} but enhanced the magnetic properties of BFO films. This suggests that the dominating factors for the increase of magnetization in BFO films are not only the existence of Fe^{2+} but also some others which may destroy the spatially inhomogeneous spin-modulated incommensurate structure to release ferromagnetism, or increase the spin canting angle of the Fe ion to result in the net macroscopic magnetization [8,29]. The Ce doping decreased the content of Fe^{2+} but enhanced the magnetic properties of the BFO films, which is consistent with our previous results and might be attributed to the suppression of the inhomogeneous spin structure of the BCFO films due to the structural transition [22,28]. Noting that the Zr doping and Ce-Zr codoping have also induced the structural transition, as mentioned in the XRD analysis above, the structure transition may also be the main cause for the increase of magnetization in the BFZO and BCFZO films. Besides, noting that the BCFO film has the lowest Fe^{2+} content and the BCFZO film has the highest Fe^{2+} content among the doped BFO films, it can be deduced that the high-valence Zr^{4+} substitution for the Fe^{3+} would produce more Fe^{2+} ions due to the charge compensation [30]. Therefore, it could be deduced that the combined action of the suppression of the inhomogeneous spin structure due to the structural transition and the formation of Fe^{2+} ions resulted in the strongest magnetization of the BCFZO film among the films studied.

In summary, the BFO, BCFO, BFZO, and BCFZO films were successfully prepared on $Pt/Ti/SiO_2/Si$ substrates by chemical solution deposition. The XRD revealed that the structural transition existed in the Ce- and Zr-doped BFO films and dense surfaces with smaller grain sizes were observed in the BCFZO film. Compared with the other doped BFO films studied here, the BCFZO film showed the lowest dielectric loss and leakage current density, as well as a well-squared P-E loop and fatigue-free characteristics. Under an applied electric field of 933 kV/cm, this film showed a remanent polarization P_r of 64 μC/cm^2 and a coercive electric field E_c of 339 kV/cm, while this film shows the strongest ferromagnetism. These improvements in ferroelectricity and ferromagnetism in this film might be attributed, respectively, to the decrease of the oxygen vacancies and the suppression of the inhomogeneous spin structure as well as the increase of Fe^{2+} in the film due to the Ce-Zr codoping.

* * *

This work was supported by the National Natural Science Foundation of China (Grant No. 50872097) and the National Key Basic Research and Development Program of China (Grant No. 2006CB932305).

REFERENCES

[1] Wang J. *et al.*, *Science*, **299** (2003) 1719.
[2] Eerenstein W. *et al.*, *Science*, **307** (2005) 1203.

[3] Catalan G. and Scott J. F., *Adv. Mater.*, **21** (2009) 2463.
[4] Wang K. F., Liu J. M. and Ren Z. F., *Adv. Phys.*, **58** (2009) 321.
[5] Smolenskii G. A. and Chupis I. E., *Sov. Phys. Usp.*, **25** (1982) 475.
[6] Ederer C. and Spaldin N. A., *Phys. Rev. B*, **71** (2005) 060401.
[7] Wang Y. and Nan C. W., *Appl. Phys. Lett.*, **89** (2006) 052903.
[8] Sosnowska I. *et al.*, *J. Phys. C.*, **15** (1982) 4835.
[9] Popov Y. F. and Kadomtseva A. M. *et al.*, *Ferroelectrics*, **162** (1994) 135.
[10] Huang F. Z. and Lu X. M. *et al.*, *Appl. Phys. Lett.*, **89** (2006) 242914.
[11] Hu G. D. and Cheng X. *et al.*, *Appl. Phys. Lett.*, **91** (2007) 232909.
[12] Yu B. F. and Li M. Y. *et al.*, *Appl. Phys. Lett.*, **93** (2008) 182909.
[13] Singh S. K. *et al.*, *Electrochem. Solid-State Lett.*, **11** (2008) G30.
[14] Murari N. M. *et al.*, *J. Appl. Phys.*, **105** (2009) 084110.
[15] Murari N. M. *et al.*, *J. Appl. Phys.*, **106** (2009) 014103.
[16] Wang Y. and Nan C. W., *Ferroelectrics*, **357** (2007) 172.
[17] Simões A. Z. *et al.*, *J. Alloys Compd.*, **479** (2009) 274.
[18] Lee S. U. *et al.*, *Appl. Surf. Sci.*, **254** (2007) 1493.
[19] Lee C. C. and Wu J. M., *Electrochem. Solid-State Lett.*, **10** (2007) G58.
[20] Cheng Z. X. *et al.*, *Phys. Rev. B*, **77** (2008) 092101.
[21] Yu B. F. and Li M. Y. *et al.*, *J. Phys. D: Appl. Phys.*, **41** (2008) 065003.
[22] Liu J. and Li M. Y. *et al.*, *J. Phys. D: Appl. Phys.*, **42** (2009) 115409.
[23] Shannon R. D., *Acta Cryst*, **32** (1976) 751.
[24] Kawae T. and Terauchi Y., *Appl. Phys. Lett.*, **94** (2009) 112904.
[25] Hwang C. S. *et al.*, *J. Appl. Phys.*, **85** (1999) 287.
[26] Zhang L. X. and Ren X. *et al.*, *Phys. Rev. B*, **73** (2006) 094121.
[27] Hu G. D. and Fan S. H. *et al.*, *Appl. Phys. Lett.*, **92** (2008) 192905.
[28] Liu J. and Li M. Y. *et al.*, *J. Alloys Compd.*, **493** (2010) 544.
[29] Bea H. *et al.*, *Philos. Mag. Lett.*, **87** (2007) 165.
[30] Hu Z. Q. and Li M. Y. *et al.*, *J. Phys D: Appl Phys.*, **42** (2009) 185010.